Determination of the Jones-Wilking-Lee – Equation of State parameters from Height-of-Burst Detonation Tests using Optimization method

A. Prado[1*]; R. Castedo[2]; A. P. Santos[2]; M. Chiquito[2]; C. Gómez-De-Cabo[2,3]; L.M. López[2]; J.I. Yenes[4].

[1] Czech Academy of Sciences, Institute of Thermomechanics, Dolejškova 5, Prague 182 00, Czech Republic.

[2] E.T.S.I. Minas y Energía – Universidad Politécnica de Madrid, C/ Ríos Rosas, 21, 28003, Madrid, Spain.

[3] Unidad de Exenciones REACH y Laboratorios de la Defensa / Área de Regulación Industrial / Subdirección General de Inspección y Regulación (SDG INREG) / Dirección General de Armamento y Material (DGAM), C/ Donoso Cortés, 92, 28015, Madrid, Spain.

[4] Escuela Politécnica Superior del Ejército – Ministry of Defense, C/ Joaquín Costa, 6, C.P. 28071, Madrid, Spain.

[*] Corresponding author:
e-mail: prado@it.cas.cz

ABSTRACT

This work presents a practical and general methodology for determining Jones–Wilkins–Lee (JWL) Equation of State (EOS) parameters through numerical optimization, which is demonstrated here for the military explosive PG3 (similar to C4). The approach couples the Sequential with Domain Reduction strategy implemented in LS-OPT with a two-dimensional axisymmetric LS-DYNA model used to simulate height-of-burst spherical air-blast detonations. Three charge weights (0.7, 1.0, and 1.4 kg) were tested, with pressure sensors placed radially at 2, 4, and 8 meters. Pressure–time histories from the 2 m and 4 m sensors of the 0.7 kg and 1.4 kg tests were used for calibration, while the 1.0 kg case and 8 m sensors were left for validation.

The optimized JWL parameters reproduced the experimental overpressures in LS-DYNA with errors mostly below ± 10 %, accurately capturing both the shape and magnitude of the positive phase. These parameters were further validated using Viper::Blast software, achieving good agreement in peak pressures and impulses.

Overall, the study demonstrates a simple and cost-effective alternative to traditional methods, such as the cylinder test, for determining EOS parameters. By relying only on basic air blast tests and numerical optimization, the proposed methodology significantly reduces experimental complexity while maintaining high predictive accuracy, making it well suited for a wide range of blast modelling applications.

Keywords: Blast simulation, LS-DYNA, JWL-EOS, LS-OPT.

1. Introduction

An Equation of State (EOS) is a mathematical expression that describes the thermodynamic behaviour of a material by relating variables such as volume, temperature, pressure, density, or internal energy. A wide variety of EOS formulations are currently available for explosives (e.g., Ignition and Growth, Mie–Grüneisen, Polynomial, Ideal Gas, among others), many of which are based on empirical or semi-empirical relationships tailored to specific material behaviours. In the context of explosion engineering, accurately defining the EOS of gaseous detonation products is critical for predicting the effects of explosions on various targets in both civilian and military applications. These equations can be implemented in advanced numerical simulation tools such as AUTODYN [1] or LS-DYNA [2], enabling high-fidelity modelling of explosive phenomena across a broad range of scenarios. Among the available EOS models, the Jones–Wilkins–Lee (JWL) equation [3] is particularly prominent due to its well-established performance in representing the expansion of detonation gases, and its widespread use in the scientific literature [4,5,6]. In parallel, the Ignition and Growth (I&G) model has been used for simulating the complete detonation process in high explosives, especially where initiation and reaction kinetics are of interest [7,8]. The I&G model captures the transition from ignition to sustained detonation through a set of rate laws that govern the evolution of pressure and energy release, making it especially suitable for reactive flow simulations involving heterogeneous explosives or complex initiation mechanisms. However, its implementation is considerably more demanding, as it requires detailed calibration of kinetic parameters and a deep understanding of the materials reaction behaviour under varying conditions.

The conventional method for determining JWL EOS typically involves conducting the cylinder test [9], followed by manual calibration of the equation parameters until the discrepancy between numerical and experimental results falls below a predefined threshold [10,11]. However, this process is often time-consuming, expensive, experimentally complex, and poses safety risks, prompting the development of alternative methods such as empirical fitting functions [12], computational techniques [13], analytical models [14,15], and optimisation algorithms [16]. For instance, Itoh et al. [17] and Li et al. [18] successfully derived the JWL parameters by analysing the shock wave generated in underwater explosive charge tests. Similarly, Bornstein et al. [5] employed an inverse modelling approach, combining field cylinder tests with numerical simulations in LS-DYNA to estimate the JWL parameters. These parameters significantly influence shock wave characteristics, including peak pressure, impulse, and time of arrival [19].

When the explosive EOS is unknown or difficult to determine, its behaviour can be approximated by using mass equivalence relative to a reference explosive with a well-characterized EOS. TNT is commonly used due to its extensive study and well-documented performance [20,21]. This approach allows simulating detonation effects without detailed EOS parameters of the specific explosive; however, it introduces additional uncertainty, as the equivalence depends on factors such as scaled distance, explosive geometry, experimental conditions, and observation point [22].

The aim of this study is twofold. First, a general and reproducible methodology is developed and demonstrated for the identification of JWL EOS parameters directly from

height of burst blast tests using an LS OPT/LS DYNA optimization framework. This methodology constitutes an alternative to the traditional cylinder test and is intended to reduce experimental complexity, cost, and safety risks while enabling systematic calibration based on field measured positive phase blast parameters. Second, the proposed methodology is applied to the military explosive PG3, for which no validated JWL EOS has been reported in the literature. PG3 is selected as a representative case study due to its compositional similarity to C4 type formulations and its operational relevance. The resulting optimized JWL parameters are subsequently implemented in the Viper::Blast CFD code to validate the methodology against experimental peak pressure and impulse measurements across different charge weights and sensor locations.

2. Jones–Wilkins–Lee (JWL) Equation Of State (EOS)

An EOS enables accurate characterisation of an explosive's behaviour by modelling the response of its detonation products immediately after the explosion.

The JWL–EOS was first described by Lee et al. [3] as a means to accurately describe the behaviour of detonation products from high explosives. Developed at Los Alamos National Laboratory (USA), the JWL–EOS provided a practical and robust model to capture the pressure and volume relationships during the initial shock compression and subsequent expansion phases of explosive gases. Since its inception, the JWL–EOS has become a fundamental tool in numerical simulations of explosive events within defence and engineering applications [24].

The JWL-EOS, as defined in Eq. (1), is widely used across a broad range of applications, offering reliable and accurate predictions. In this study, optimisation techniques are used to identify its unknown parameters.

$$P = A\left(1 - \frac{\omega}{R_1 V}\right)e^{-R_1 V} + B\left(1 - \frac{\omega}{R_2 V}\right)e^{-R_2 V} + \frac{\omega E}{V} \quad (1)$$

Where P is the pressure of the system, V corresponds to the relative volume, defined as $V = v/v_0$, the energy term E includes both the chemical bond energy, and the kinetic energy associated with the momentum aspect of the flow. A, B, R_1, and R_2 are constants, where A and B are related to the initial pressure of the detonation gases, and R_1 and R_2 govern the decay rate of the exponential terms as a function of the relative volume of the detonation products. ω represents the volumetric expansion associated with the adiabatic coefficient (γ) of ideal gases, such that $\omega = \gamma - 1$. This parameter describes how the pressure and internal energy of the gas are related during the expansion of the detonation products.

Despite its widespread use and robustness, the JWL also has limitations that must be considered. One key assumption of the JWL formulation is that the explosive undergoes an ideal detonation, where a steady Chapman-Jouguet (CJ) state is reached immediately behind the detonation front [24]. This assumption makes it particularly well-suited for high-performance military explosives, which typically conform to ideal detonation theory. However, it may not accurately capture the behaviour of non-ideal or low-velocity

explosives, such as ammonium nitrate/fuel oil (ANFO) or emulsion-based charges, which are widely used in civil engineering and mining applications.

In such cases, alternative EOS, such as the Ignition and Growth (I&G) model [25], may provide better predictions. The I&G model accounts for non-ideal behaviour by introducing empirical terms that model the ignition, growth, and completion phases of the reaction zone, enabling a more realistic description of the pressure-time evolution. However, this model is significantly more complex, requires a greater number of parameters, often difficult to obtain without extensive experimental data.

A commonly used experimental technique to validate EOS models, in particular the JWL, is the cylinder test [3]. In this test, a cylindrical explosive charge is confined within a metal tube, and upon detonation, the radial expansion of the tube is measured using high-speed diagnostics. From this, pressure-volume (P–V) data of the detonation products can be determined. The expansion curve obtained from the cylinder wall motion is typically used to fit the JWL parameters, especially the constants A, B, R_1, R_2, and ω, which describe the pressure decay and energy release of the explosive gases. However, this test requires a complex experimental setup and involves a high economical cost.

3. Tests Description

In 2022, a series of height-of-burst detonation tests were carried out at the *Palancar Firing Range, Hoyo de Manzanares*, using the military explosive PG3, developed by the Spanish company EXPAL. This product is composed of 89 % cyclotrimethylenetrinitramine (RDX), a compound widely used in the military industry, and 11 % hydroxyl-terminated polybutadiene (HTPB), a plastic additive. The resulting compound has a density of 1580 kg/m³.

A total of ten blast tests were conducted: four with a 1.4 kg charge, three using a 1 kg charge and three with a 0.7 kg charge (as presented in Table 1). An additional test was performed with the 1.4 kg charge to compensate for a malfunction in one of the pressure sensors during one of the trials. This repetition ensured the accuracy and completeness of the experimental dataset.

Table 1. Explosive charges used in the tests.

Test	Explosive Mass PG3 (kg)	Charge Radius (cm)
T1, T2, T3 and T4	1.4	5.96
T5, T6 and T7	1	5.33
T8, T9 and T10	0.7	4.73

Each test involved a spherical explosive charge initiated in its centre and suspended 0.5 meters above the ground. Pressure sensors (PCB Piezotronics®), with a measurement range of 3.45×10^5 to 3.45×10^6 Pa, were positioned at radial distances of 2 meters (S1 and S2), 4 meters (S3 and S4) and 8 meters (S5 and S6) from the charge. Fig. 1 shows a schematic of the experimental setup. The pressure sensors were factory-calibrated and periodically recalibrated according to the manufacturer recommendations. A calibration check was performed before the test campaign to ensure consistency among sensors. Fig.

2 presents photographs taken before the detonation, while Fig. 3 shows the expansion of the shockwave.

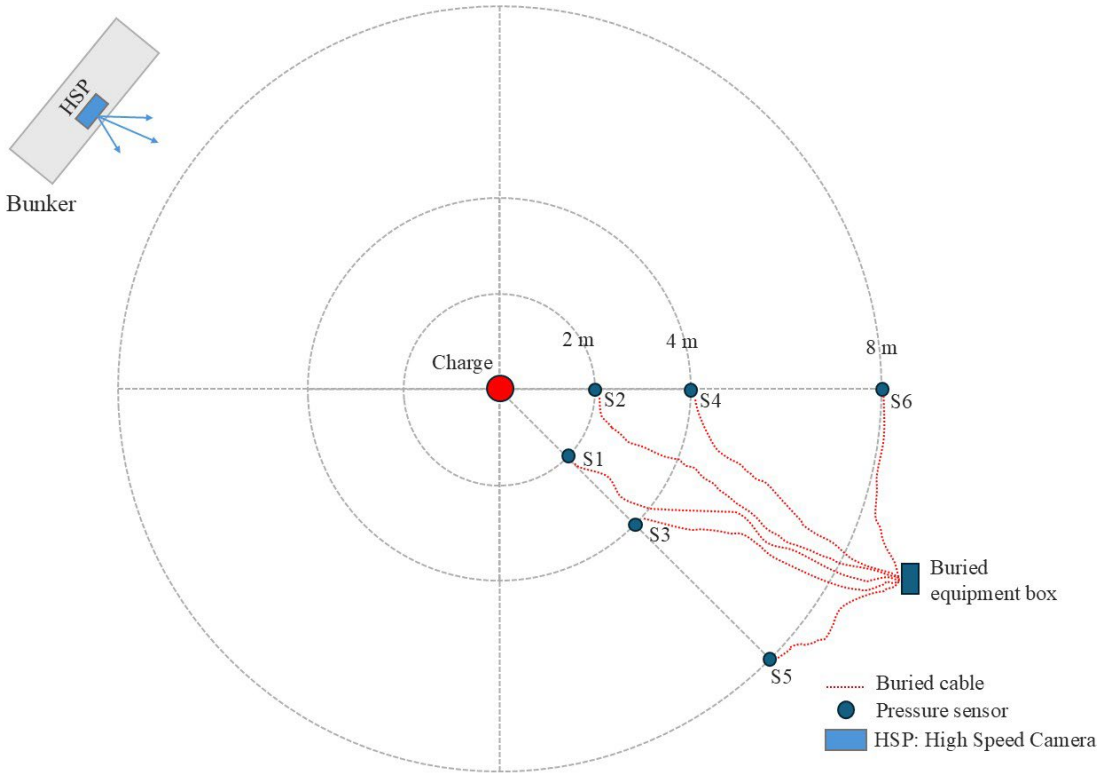

Fig. 1. Test configuration. The distance of the bunker is not to scale, as it is located at 65 from the charge.

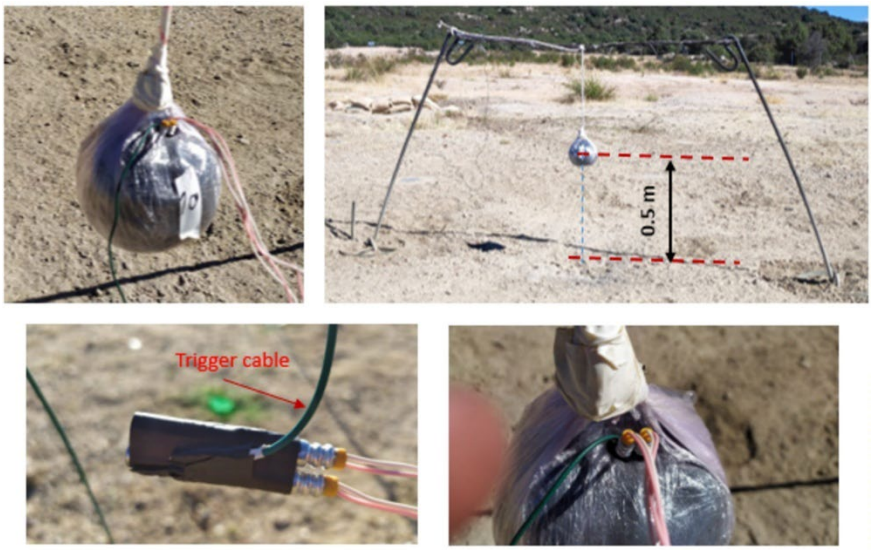

Fig. 2. Photographs of the explosive charge. Initiation and location.

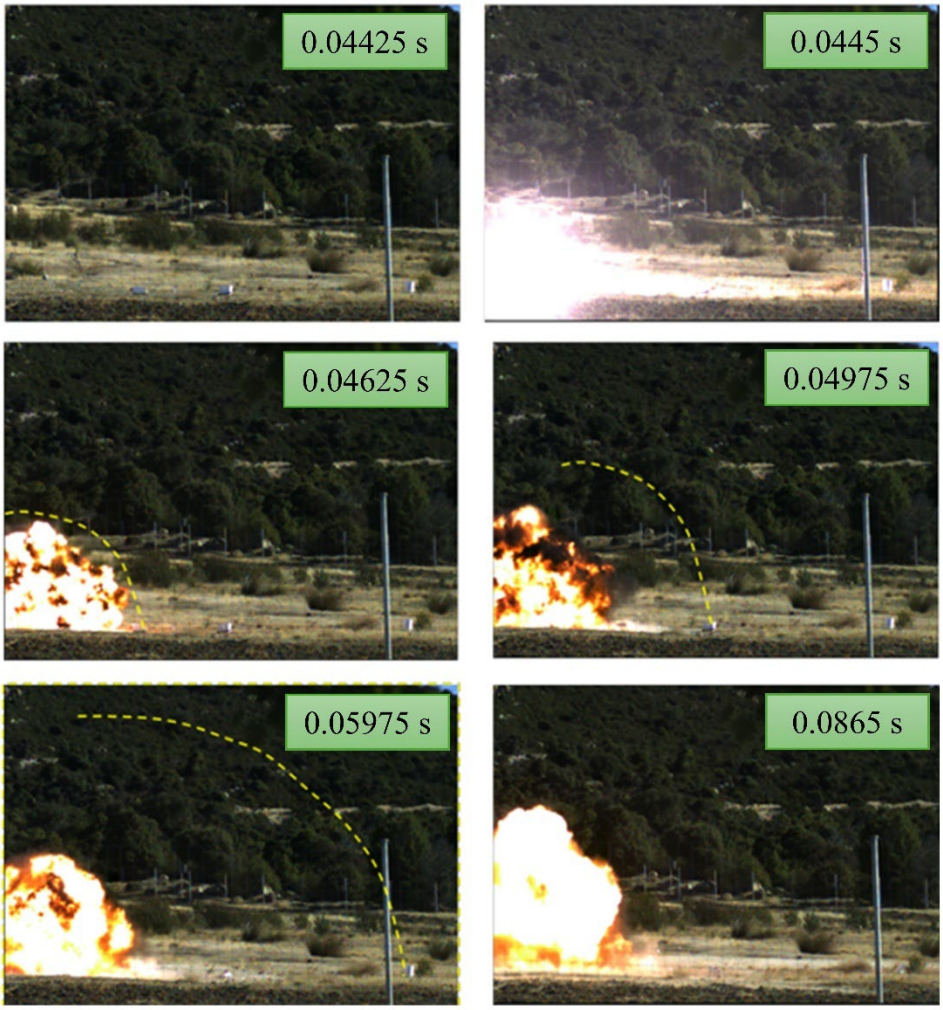

Fig. 3. Photographs of the expanding shockwave (test T5).

The pressure signals recorded by the sensors were first processed to remove noise using a fourth-order Butterworth low-pass filter. When necessary, an offset correction was also applied, as done by Chiquito et al. [23]. As example, the original and filtered signal for sensor S1 in test T8 (0.7 kg charge) are shown in Fig. 4.

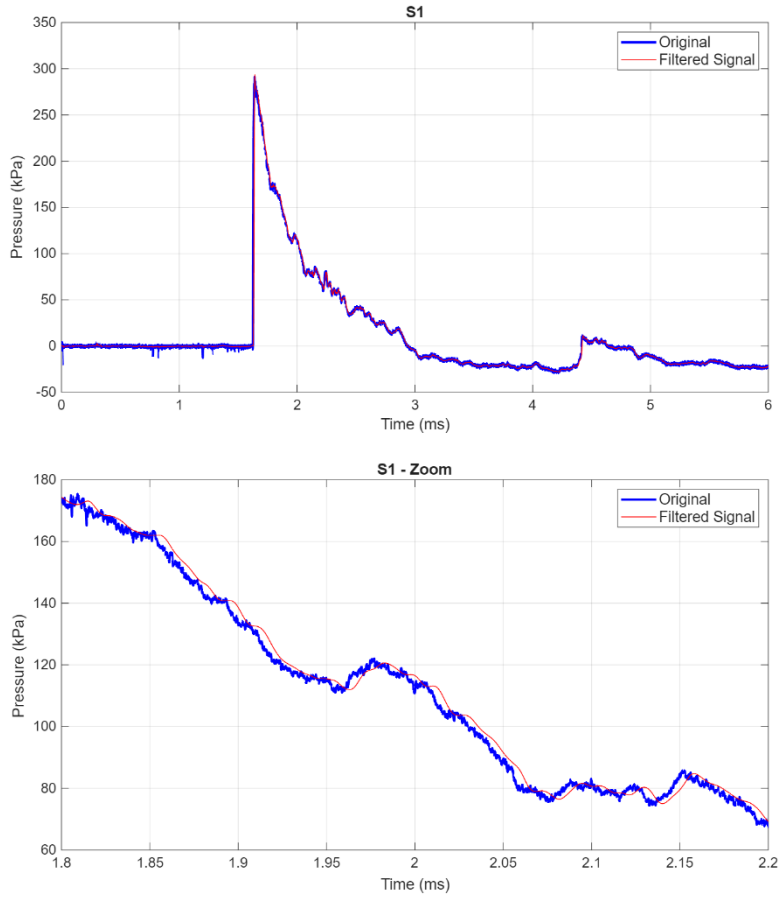

Fig. 4. Original and filtered pressure–time signals for sensor S1 in test T8, corresponding to 0.7 kg charge.

The filtered signals were then fitted to the Friedlander equation (see Eq. (2)) [26,27], in order to extract the key parameters of the positive phase of each test.

$$p(t) = p_{max} \cdot (1 - \frac{t}{t_d}) \cdot e^{-b \cdot t / t_d} \quad (2)$$

Where $p(t)$ is the pressure as a function of elapsed time, p_{max} is the maximum pressure, t_d is the positive phase duration and b is the coefficient that describes the rate of decay of the pressure-time curve, known as the waveform or decay parameter. A graphical example of the fit to the Friedlander equation is shown in the Fig. 5 for Test 1 (1.4 kg), sensor S1. These approximations were carried out to improve the robustness of the optimisation process by reducing the influence of experimental noise and enabling the extraction of physically meaningful parameters, thus allowing more consistent comparisons with the simulated results [28].

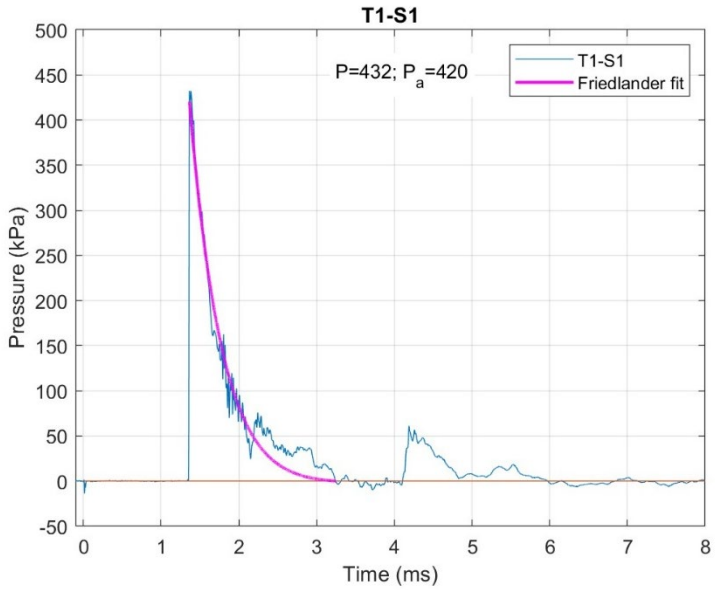

Fig. 5. Fitting of the pressure signal to the Friedlander equation for Sensor S1 in Test 1 (1.4 kg).

4. Numerical Modelling

A two-dimensional axisymmetric model was developed using the Arbitrary Lagrangian-Eulerian Multimaterial (MM-ALE) technique in LS-DYNA, as this method is particularly well-suited for simulating problems involving both fluids and solids under highly dynamic conditions. The MM-ALE approach effectively combines the advantages of Lagrangian and Eulerian formulations, allowing for accurate tracking of fluid motion, such as air movement, while avoiding excessive mesh distortion typical of purely Lagrangian analyses [29]. Moreover, it offers greater computational efficiency, which is essential for iterative processes requiring multiple simulations [30]. This LS-DYNA model serves as the foundation for the optimization process performed in LS-OPT, where selected parameters are calibrated based on the numerical results obtained from the simulations.

The geometry of the model used to represent the field test is shown in Fig. 6(A). A structured mesh of square elements with a side length of 1.25 cm was employed, offering an appropriate compromise between numerical accuracy and computational cost. The mesh size was selected based on the criteria established in [29], where a grid sensitivity analysis based on the Grid Convergence Index (GCI) methodology is defined and applied. In that study, three different refined meshes with a constant refinement ratio were analysed, allowing the order of convergence to be estimated and the numerical solution to be verified as lying within the asymptotic convergence range. The resulting GCI values demonstrated that the selected mesh resolution provides mesh-independent pressure–time responses within a 95 % confidence bound for the near- and mid-field blast regime considered in the present work.

In the area surrounding the detonation (Fig. 6(B)), two distinct mesh geometries were implemented. In the region closest to the explosive, square elements of 0.277 cm were

used to achieve greater resolution in this critical zone. This high-resolution area is aligned with the centre of the explosive. Moving outward from this central region, a "butterfly" meshing pattern was applied, as it has proven highly effective for modelling the detonation of spherical explosive charges [27,31]. Furthermore, mesh refinement was applied at the sensor positions to improve accuracy, as shown in Fig. 6 (C) for sensors S3 and S4.

This mesh configuration provides reliable results for sensor locations at 2 m and 4 m, where the blast wave is still relatively strong and well resolved by the numerical discretisation. At 8 m, however, the propagated shock wave is significantly weaker, with reduced pressure gradients and increased sensitivity to numerical diffusion. Under these conditions, numerical errors and discretisation limits associated with the selected mesh accumulate, making the pressure signal unusable. While the mesh could in principle be refined to improve accuracy at this distance, doing so would substantially increase computational time and compromise the accuracy at closer sensor locations, deviating from the mesh resolution validated through the GCI analysis. For this reason, the 8 m sensor was excluded from the LS-DYNA simulations and used instead for validation with the Viper::Blast software.

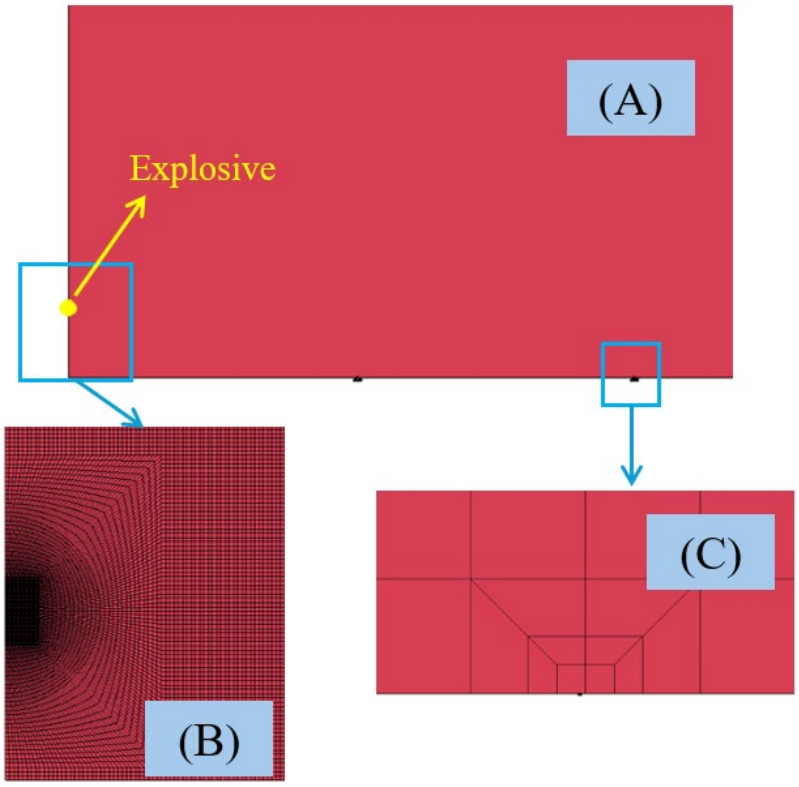

Fig. 6. Schematic of the 2D numerical model employed (A) with mesh detail in (B) and (C).

Boundary conditions were applied to the bottom face, representing the ground, constraining both its translation and rotation to fully fix the model in space. The ground reflects the pressure wave, while the remaining boundaries are treated as non-reflecting. The top and right boundaries (see Fig. 6) were positioned sufficiently far from the charge

to avoid undesired reflections, which can still occur even when non-reflecting boundary conditions are employed.

Only two materials are involved in the model: air and the explosive (PG3). Air was modelled as an ideal gas using the **Mat_Null* material card, with a density of 1.29 kg/m³ and all other parameters set to zero. Its EOS was defined using the **Linear_Polynomial* card, as expressed in Eq. (3).

$$P = C_0 + C_1\mu + C_2\mu^2 + C_3\mu^3 + (C_4 + C_5\mu + C_6\mu^2)E \quad (3)$$

Where P is the pressure, C_0, C_1, C_2, C_3, C_4, C_5, and C_6 are constants, μ is defined as $\rho/\rho_0 - 1$ (with ρ being the density previously specified in **Mat_Null*), and E is the internal energy per unit volume. The parameters C_4 and C_5 are set to 0.4, E is defined as 0.25 MPa, the specific volume (V_0) is taken as 1, and all remaining parameters are left as default [7,32].

To define the explosive PG3, the input cards and data presented in Table 2 were used. Parameters marked with an asterisk indicate those to be identified through the optimisation process. The parameters selected for optimisation were incorporated using the **Parameter_Parameter* card, enabling their calibration.

Table 2. Input cards and corresponding data used for the definition of explosive PG3. **EOS_JWL* parameters correspond to those in Eq. (1).

*Mat_High_Explosive_Burn					
Density (kg/m³)		Detonation velocity (m/s)		Chapman-Jouguet pressure (GPa)	
1580		8238		25.68	
*EOS_JWL					
A (Pa)	B (Pa)	R_1	R_2	ω	E_0 (GPa)
*	*	*	*	0.37	8.611

The density value corresponds to that provided in the technical data sheet of the explosive. In the case of the detonation velocity, the value of 8238 m/s was obtained through thermodynamic calculations using the W-DETCOM code [32]. This approach was chosen as it is considered the most accurate under the specific conditions of this study, providing a detonation velocity consistent with the explosive's actual properties, and ensuring coherence with the thermodynamic parameters used in the simulations. The Chapman-Jouguet pressure (P_{CJ}) was also calculated using the same thermodynamic code.

The parameter E_0 has been calculated using the heat of explosion (Q = 5,450 kJ/kg) and the density of the PG3 (see Eq. (4)).

$$E_{0_{max}} = Q \cdot \rho \quad (4)$$

This calculation yields the value of $E_{0_{max}} = 8.611\ GPa$.

In the case of ω, a curve is fitted to the pairs of values V (specific volume) and γ (volumetric expansion coefficient), see Fig. 7. These data are obtained from the isentropic expansion calculated with W-Detcom. The fitting follows the form of Eq. (5).

$$f(x) = a \cdot e^{-bx} + c \quad (5)$$

From this equation, the constant term is extracted, which allows the calculation of the parameter ω, following the expression: $\omega = c - 1$. The fit can be seen graphically in Fig. 7, from which a value of ω = 1.37 – 1 = 0.37 is obtained.

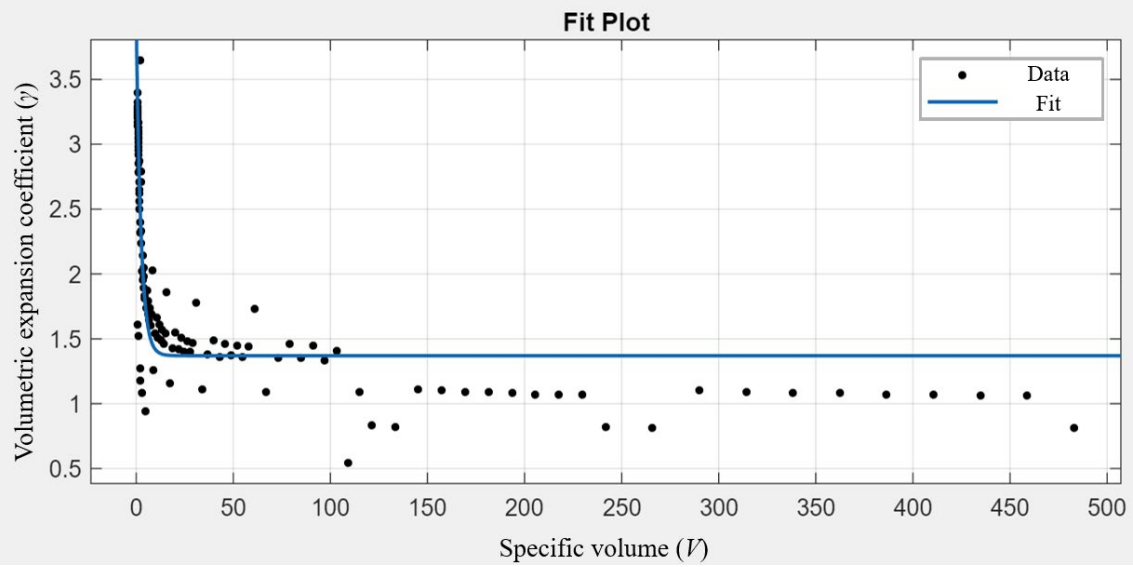

Fig. 7. Graph of the curve fitted to the $V - \gamma$ data points, with variables expressed in SI units.

5. Optimization Procedure

The optimisation process was carried out using the LS-OPT software, a standalone graphical optimisation tool specifically designed for use with LS-DYNA. In this study, LS-OPT was employed to identify the unknown parameters of the JWL-EOS, which are critical for accurately simulating explosive behaviour, as detailed in Table 2. Note that, since no published and validated JWL-EOS exists for PG3, the optimization does not start from any predefined or "baseline" parameter set. Instead, it directly identifies the coefficients A, B, R_1, and R_2 that minimize (under explicit weighting) the discrepancies in peak overpressure and in the morphology of the positive phase, as estimated through a Friedlander fit applied to the filtered experimental pressure records. This choice is fully consistent with the objective of proposing a methodology that is both reproducible and extensible to other explosive formulations, rather than merely performing an incremental update of existing parameter sets.

Similar approaches can be found in the literature. For example, in Yi et al. [8], LS-OPT was combined with LS-DYNA to calibrate the parameters of the I&G model for aluminized emulsion explosives, based on data from confined detonation tests to measure front curvature and velocity. Likewise, Bergh et al. [34] presented a procedure for calibrating the I&G model for PBXN-109, using hydrocode simulations in conjunction with LS-OPT. Their work included cylinder expansion tests, a new automatic routine for EOS calibration, and rate stick and gap tests for burn model parameter estimation.

In this work, a maximum of 20 iterations was specified, employing the Sequential Response Surface Method (SRSM) strategy within LS-OPT. While other optimization algorithms exist within LS-OPT, SRSM and Efficient Global Optimization (EGO) are the most robust. However, EGO is limited to scalar objectives and cannot accommodate the set of points defining the positive phase of the pressure wave, which are required as target values in this study. SRSM was therefore selected for its robustness and compatibility with the objectives of this study. The SRSM approach utilises metamodel-based optimisation, which constructs an approximate surrogate model based on a limited set of computationally expensive, high-fidelity simulations. The optimisation is performed on this surrogate to efficiently explore the parameter space. At each iteration, new sample points are adaptively added within a progressively reduced subregion, improving the surrogate model's accuracy and focusing the search for the global optimum [35]. This iterative refinement not only accelerates convergence but also significantly reduces the computational cost compared to direct optimisation methods.

Two separate LS-DYNA models were incorporated into the optimisation framework, representing explosive charges of 0.7 kg and 1.4 kg. These models recorded pressure–time histories at sensor locations positioned 2 m and 4 m from the blast centre. Importantly, the 1 kg charge was reserved solely for validation purposes. Likewise, the pressure sensors located 8 m from the blast centre were used for validation in Viper::Blast. This decision was motivated by the computational challenges of obtaining reliable pressure results at such large distances in LS-DYNA, given the mesh size and configuration employed in this study.

In Fig. 8, the four variables of the JWL-EOS to be determined are defined within the "Sampling 1" box. The two models are then executed, and their outputs are evaluated in the "Composites" box, which corresponds to the peak pressure and the nine values of the positive phase (explained below) measured at 2 m and 4 m for each simulation, resulting in a total of eight definitions.

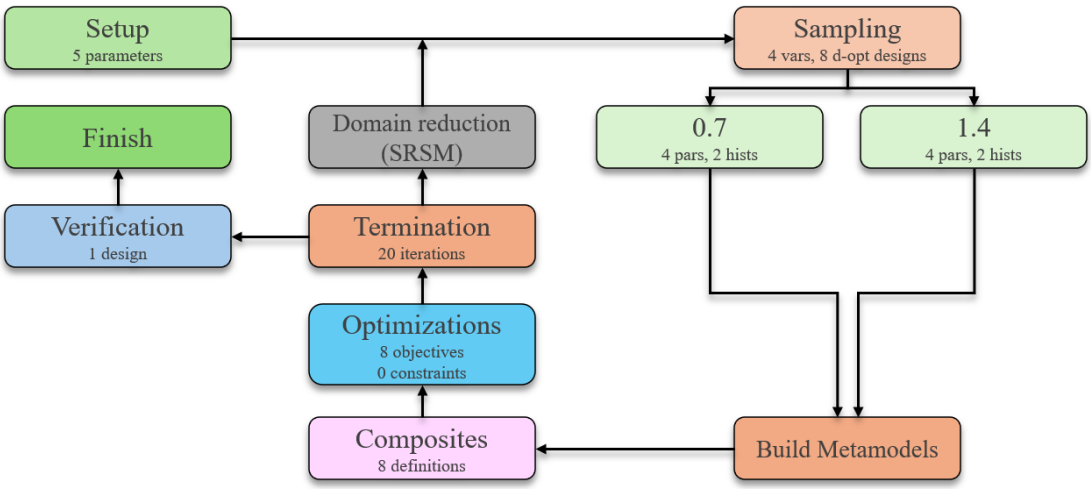

Fig. 8. General scheme of the optimisation process carried out using LS-OPT. "0.7" and "1.4" refer to the 0.7 kg and 1.4 kg PG3 models, respectively.

The optimisation procedure seeks to minimise the discrepancy between simulated and experimental results, quantified through the Mean Squared Error (MSE). Generally, the

MSE for a set of predictions $\hat{y}_i$ compared against observed values y_i over N data points is defined as in Eq. (6):

$$MSE = \frac{1}{N} \cdot \sum_{i=1}^{N} (y_i - \hat{y}_i)^2 \quad (6)1$$

In this study, the MSE formulation is adapted to simultaneously account for two key output variables: the peak pressure and the shape of the positive phase of the pressure-time curve, sampled at 10 time points: the first point corresponds to the peak pressure, while the remaining nine points are equally spaced in time over the duration of the positive phase. These values were obtained from the average Friedlander equation, derived using the three valid tests performed for each explosive charge. To emphasize peak pressure during the optimization process, 50 % of the weight is assigned to the first point (the pressure peak), while the remaining 50 % is equally distributed among the other nine points, which form the shape of the positive phase. Since two pressure sensors are available at each distance, the average of the corresponding time series is used for model calibration. The objective function $J(p)$, dependent on the vector of JWL parameters p, is defined as shown in Eq. (7):

$$J(p) = \frac{1}{N_s} \sum_{i=1}^{N_s} \left[w_1 \cdot \left(\frac{P_{sim,i}(p) - P_{exp,i}}{P_{exp,i}} \right)^2 + w_2 \cdot \left(\frac{A_{sim,i}(p) - A_{exp,i}}{A_{exp,i}} \right)^2 \right] \quad (7)$$

where:

- N_s is the number of sensor measurements considered.
- $P_{sim,i}(p)$ and $A_{sim,i}(p)$ represent the simulated peak pressure and pressure points from the positive phase at sensor i.
- $P_{exp,i}$ and $A_{exp,i}$ are the corresponding experimental values.
- w_1 and w_2 are weighting factors assigned to peak pressure and average positive phase errors, respectively (equal weights are used in this work).

6. Optimization Results

The JWL parameters were established through an optimisation process comprising eleven iterative steps. During this procedure, the optimisation algorithm progressively refined the key coefficients A, B, R_1, and R_2, adjusting their values at each iteration to improve the fit between the model predictions and the experimental data. This iterative refinement continued until convergence criteria were met. The final calibrated values, which underpin the JWL-EOS utilised in this study, are compiled in Table 3. Examples of experimental and optimised pressure–time curves are presented in Fig. 9.

Table 3. Optimised JWL parameters obtained for PG3.

ρ_0 (kg/m^3)	P (GPa)	D (m/s)	E_0 (GPa)	A (Pa)	B (Pa)	R_1	R_2	ω
1580	25.68	8238	8.611	1.004×10^{12}	5.440×10^{9}	5.173	1.860	0.37

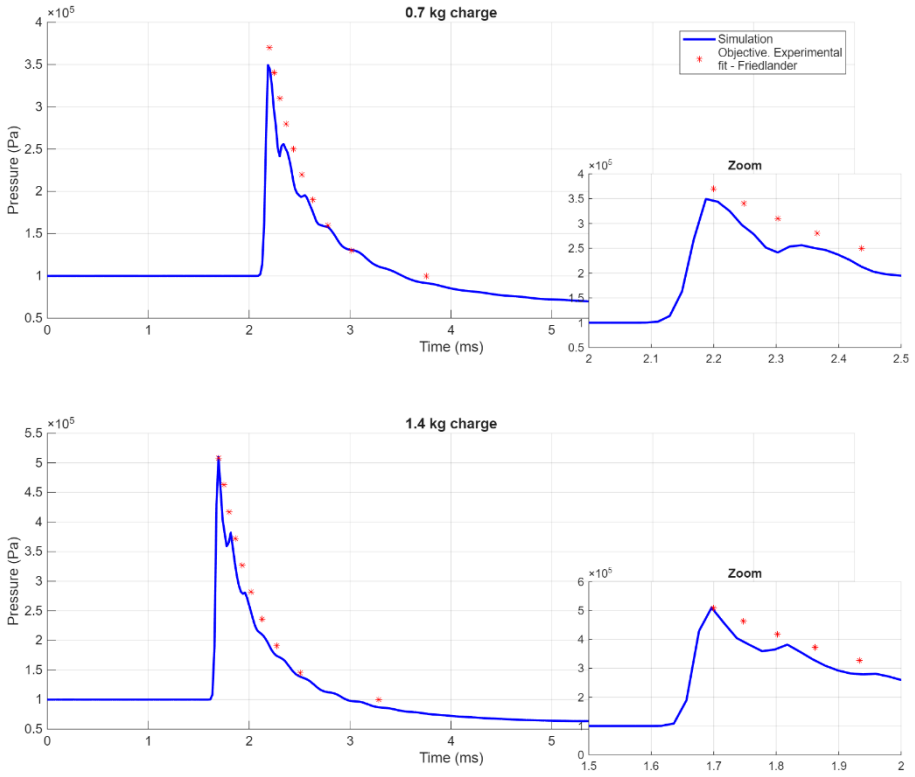

Fig. 9. Optimised pressure–time graph for sensors located at 2 m and the objective points from experimental data.

Using the calibrated JWL parameters, approximations of both the peak pressure and the average positive phase were calculated. While this average positive phase is related to the impulse, it does not represent the impulse exactly, as it is computed from only nine points along the positive phase and does not account for the entire area under the pressure curve. Table 4 summarises the findings and comparison with experimental data, with most values deviating by less than ± 10 % from those measured in field tests, regardless of the specific test conditions or sensor locations used for comparison. The largest differences are observed in the average positive phase for the 0.7 kg charge, where predicted values are approximately 10 % lower than the experimental data. This increased deviation is primarily attributed to the larger variability observed among the pressure sensors in the 0.7 kg tests compared to the 1.4 kg configuration. For smaller charges, the positive phase duration is shorter and closer to the temporal resolution and noise floor of the measurement system, making it more sensitive to inter-sensor scatter and post-processing criteria used to define the end of the positive phase. As a result, quantities such as the average positive phase exhibit greater experimental dispersion, which partially explains the larger discrepancy observed in this case. Overall, the level of agreement remains within acceptable bounds for blast modelling applications.

Table 4. Peak pressure and average relative differences of the JWL optimisation. Differences are calculated in relation to the experimental measurements, and average differences correspond to those of the positive phase in the pressure-time graph.

	0.7 kg		1.4 kg	
Differences	S1 and S2 (2 m)	S3 and S4 (4 m)	S1 and S2 (2 m)	S3 and S4 (4 m)
Peak Pressure	-6.57 %	6.19 %	-1.42 %	2.49 %
Average positive phase	-9.73 %	-10.43 %	-4.92 %	-4.40 %

A validation simulation was conducted using the same two-dimensional model employed during the optimisation phase. In this case, the optimised JWL parameters were kept fixed and applied to a test scenario that included the 1 kg charge, which had not been included in the parameter fitting process. The results demonstrate good predictive capability: peak pressure estimated at sensors positioned 2 and 4 meters from the charge exhibit relative differences of -5.57 % and 10.81 %, respectively. In addition, the average error across the nine points of the positive phase shows relative differences of 6.21 % and -3.70 %, confirming that the optimised parameters generalise well to independent test conditions. The pressure–time histories from both the experimental tests and the simulations for the 1 kg charge are presented in Fig. 10. The R^2 values for the fit between the simulations and the Friedlander fit to the experimental results at the sensors located 2 m and 4 m from the charge are 0.953 and 0.823, respectively. These R^2 values were calculated over the positive phase. The lower R^2 observed at the more distant sensor is attributed to the reduced accuracy of the simulation at greater distances, which is why the 8 m sensor was not evaluated with LS-DYNA.

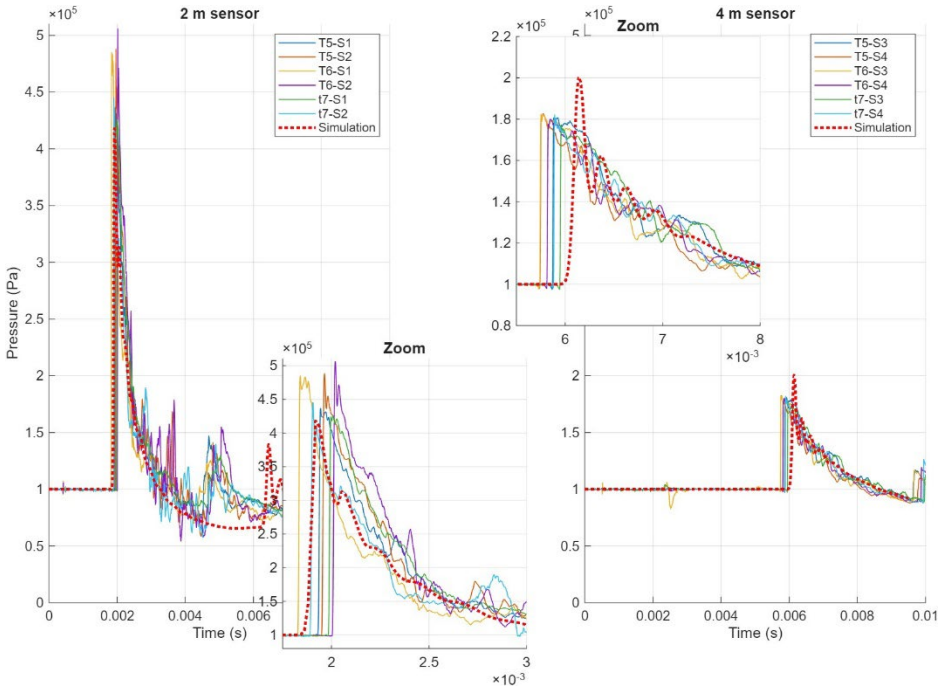

Fig. 10. Pressure–time graph for the 1 kg test – comparison of experimental and simulation results using the optimised JWL EOS.

The optimized JWL model effectively reproduces both peak pressure and the average positive phase across scaled distances ranging approximately from 1.8 to 4.5 m/kg$^{1/3}$. In the next section, the Viper software is used to validate the optimized JWL-EOS by calculating peak pressures and impulses for all tests and sensors, thereby extending the upper scaled distance range up to 9 m/kg$^{1/3}$.

7. Validation

A numerical model was built using Viper::Blast [36] to validate the results obtained. Viper::Blast is a finite volume computational fluid dynamics code for the simulation of blast effects. The numerical scheme is based on the Advection Upstream Splitting Method (AUSMDV) method, and it has further been extended to allow for the simulation of blast physics on GPU's. This leads to a significant increase in performance and scalability for problem types such as those described here.

Viper offers different approaches to solving the problem, one of which is the possibility of manually entering the equation of state for the explosive to be used. The optimized JWL-EOS parameters (Table 3) were introduced in the software, performing simulations for the 0.7, 1 and 1.4 kg tests, and recording pressure signals at 2, 4 and 8 m sensors. Peak pressures were then calculated and compared with those obtained from LS-DYNA simulations to demonstrate the complementarity of multi-software verification. The relative differences in peak pressures between Viper::Blast and LS-DYNA simulations at the 2 m and 4 m sensors were 3.59 % and –7.50 % for the 0.7 kg charge, 7.09 % and –12.46 % for 1 kg, and 12.29 % and –3.47 % for 1.4 kg, respectively. This corresponds to an average absolute difference of 7.73 % in peak pressures, which is considered a reasonably good agreement.

The simulation was conducted using a 1D – 2D approach due to the symmetry conditions of the experimental set up. The 1D simulation is used at the first stage of detonation before the shock wave reaches the ground, then remapping it into a 2D simulation. This approximation is made to achieve greater refinement of the mesh at the start of detonation, thereby obtaining more accurate results. Since the load was suspended at a height of 0.5 m, the domain of the 1D simulation is 0.49 m in radius with a cell size of 0.5 mm. The simulation is then remapped to 2D with a cell size of 0.01 m. As a visual example of the simulations, Fig. 11 presents the 2D domain with location of pressure sensors and explosive charge as well as the expansion of the blast wave.

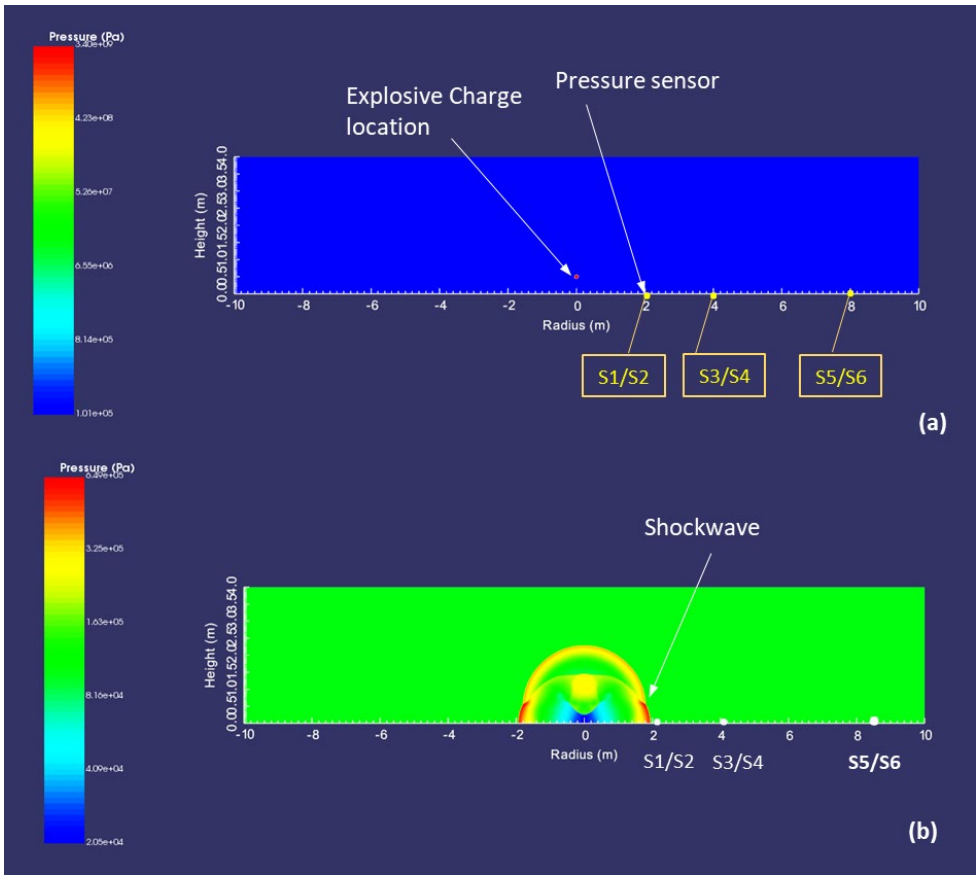

441

442 Fig. 11. Viper 2D simulation. a) Location of sensors and load; b) arrival of the shock
443 wave at sensors S1/S2 located 2m from the load.

444 To select the appropriate mesh size for the 2D simulation, a mesh sensitivity study was
445 carried out. Mesh sizes of 4, 2, 1, 0.5 and 0.2 cm were employed. The results of all tests
446 performed with 1 kg of PG3 were used for the study and compared with the modelling
447 results obtained. To evaluate the results, the parameter ε is defined as the difference in %
448 between the simulated and experimental pressure mean values for a given scaled distance,
449 according to the Eq. (8):

$$\varepsilon = \left| \frac{P_{sim} - P_{exp}}{max\{P_{sim}, P_{exp}\}} \right| \cdot 100 \quad (8)$$

450 Where P_{sim} is the simulated peak pressure, and P_{exp} is the average of the peak pressures
451 registered in the field tests. The mean values of ε, for the three sensor positions with
452 respect to the mesh size, are shown in the Fig. 12. A mesh size of 1cm leads to differences
453 between experiment and simulation of 5 % and this value stabilizes, so a mesh size of
454 1cm was selected for the study.

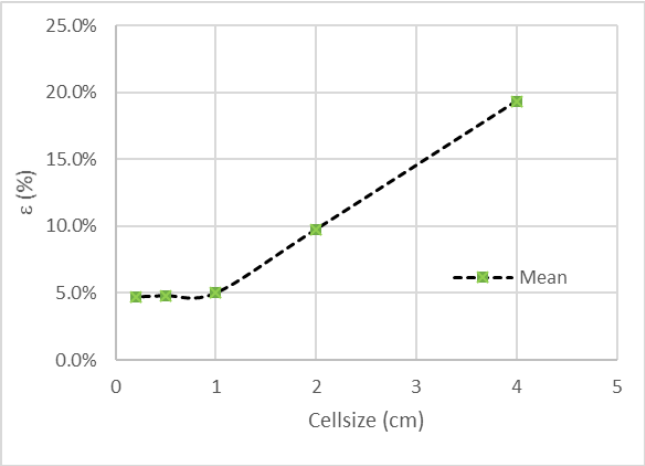

Fig. 12. Differences between experimental pressures and Viper 2D model according to mesh size (1 kg PG3 tests).

Fig. 13 shows the pressure–time signals obtained from the Viper simulations and the experimental measurements, including results computed using both the optimised PG3 JWL parameters and a standard C4 JWL parameter set (used for comparison purposes) provided by Viper::Blast [36]. Overall, both numerical models reproduce well the shape and magnitude of the measured pressure evolution. The responses obtained with the C4 and PG3 parameterisations are similar, with only a slightly earlier time of arrival and minor differences in peak pressure and impulse (less than 5 %) for the C4 model.

The close agreement between the independently calibrated PG3 model and the C4 response, despite the absence of any C4-based assumptions during calibration, supports the physical consistency and robustness of the proposed identification methodology. The main contribution of this approach is to provide a general and transferable framework for deriving reliable JWL parameters for new explosives.

Noticeable variations in arrival times were observed between different sensors, particularly for those at 2 m sensors, as well as between the sensors and the simulations. These discrepancies are attributed to experimental uncertainties, such as sensor placement and response times, together with modelling simplifications, including idealised geometry and material properties. Larger discrepancies are also observed for the second pressure wave. In height-of-burst tests, interaction of the detonation products with the surrounding air and reflecting surfaces promotes mixing and secondary combustion (afterburn), which can significantly modify the timing and magnitude of subsequent pressure waves, as reported in previous studies [37, 38]. Although the JWL-EOS does not explicitly resolve these processes, the experimental pressure histories used for calibration inherently include their influence. Consequently, the optimisation procedure does not physically model afterburn, but rather embeds its net effect in an implicit, lumped manner within the fitted JWL parameters. As a result, the calibrated parameters should be interpreted as effective, configuration-specific quantities and their applicability to other geometries, scales, or burst conditions may be limited.

The numerical relative differences between PG3 simulations and experimental data for both peak pressures and impulses are presented in Table 5 for all tests and sensors.

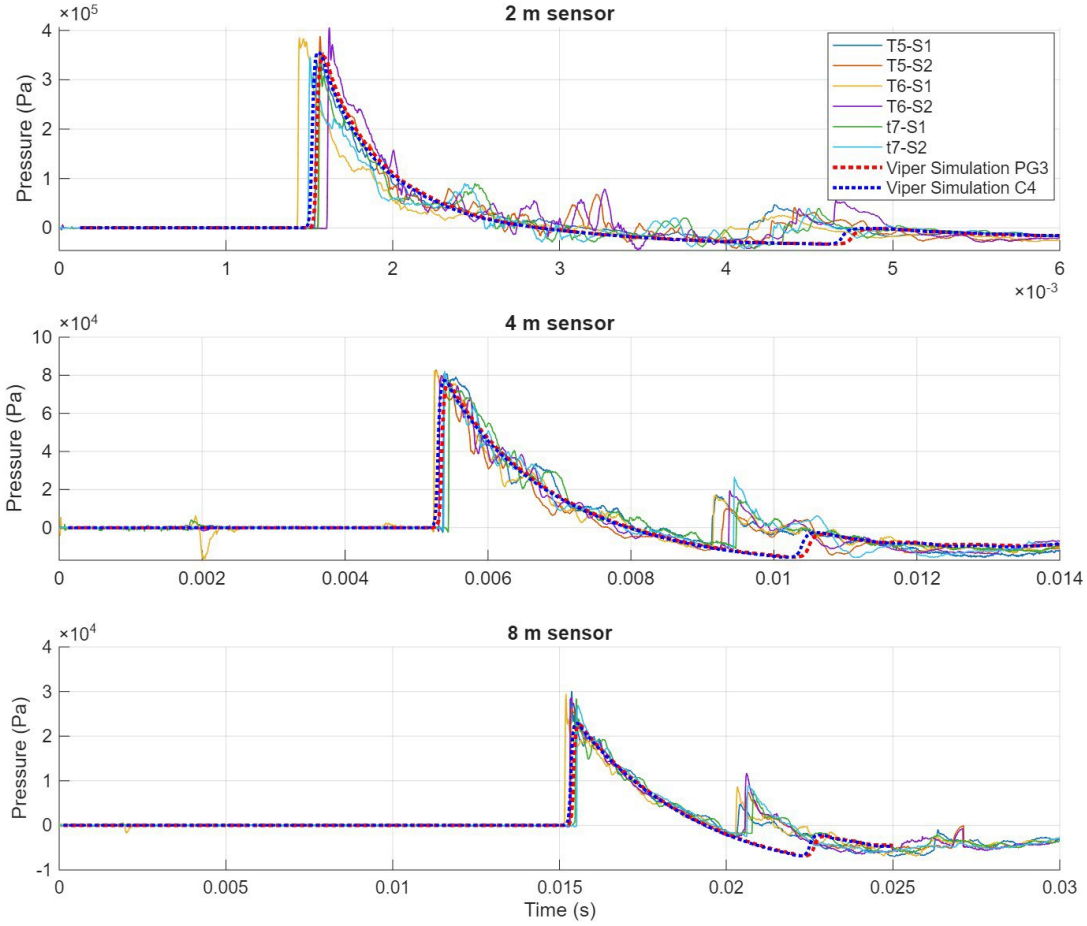

Fig. 13. Comparison of pressure–time histories between Viper simulations and adjusted field test data for 1 kg charge tests.

Table 5. Relative differences in peak pressure and impulse between the PG3 Viper simulations and the experimental measurements for all tests and sensors.

	2 m		4 m		8 m	
Test	Peak pressure (%)	Impulse (%)	Peak pressure (%)	Impulse (%)	Peak pressure (%)	Impulse (%)
0.7 kg	-4.42	-1.26	-4.58	-11.45	-7.84	-12.59
1 kg	1.42	4.57	-6.22	-5.53	-6.37	-10.46
1.4 kg	13.30	3.43	-2.12	-4.78	-5.60	-8.36

Table 5 shows the peak pressure results. Across all tests and sensors, the overall average relative difference was 5.76 %, with only one measurement exceeding 10 %. This outlier corresponds to the 2 m sensor in the 1.4 kg test, which recorded highly scattered peak pressure values across different sensors and test repetitions, ranging from 436 kPa to 565 kPa. The simulation result falls within this range, close to the upper limit. For the 0.7 kg, 1 kg, and 1.4 kg tests, the relative absolute differences were 5.61 %, 4.67 %, and 7.01 %, respectively. Regarding sensor locations at 2 m, 4 m, and 8 m, the relative absolute differences were 6.38 %, 4.30 %, and 6.61 %, respectively. These results indicate that the numerical model with the optimized JWL-EOS reliably captures the peak

pressure behaviour across different charges and sensor locations, despite some variability in individual measurements.

As for the impulse results, a global relative difference of 6.94 % was achieved, indicating good agreement between simulations and experimental data. The accuracy of the predictions improves for sensors located closer to the charge: the 2 m sensor shows a relative error of 3.09 %, while the 4 m and 8 m sensors exhibit higher errors of 7.25 % and 10.47 %, respectively. Similarly, the relative differences decrease with increasing charge mass, with values of 8.43 %, 6.86 %, and 5.52 % for the 0.7 kg, 1 kg, and 1.4 kg tests, respectively. These trends suggest that the optimised JWL-EOS is able to reliably capture the impulse distribution, particularly for larger charges and closer sensor locations, while slightly underestimating the impulse values at farther distances.

8. Conclusions

A JWL-EOS for the military explosive PG3 was obtained through an iterative process based on the Sequential with Domain Reduction method, implemented in the LS-OPT software. A two-dimensional model compatible with LS-OPT was developed in LS-DYNA to simulate the air detonation of spherical explosive charges. The optimisation process used data from six air blast tests involving 0.7 and 1.4 kg charges of PG3, with three tests conducted per charge weight. Equal weighting was assigned within the positive phase, with 50 % of the weight given to the peak pressure and the remaining 50 % distributed across the other data points defining the positive phase. The optimisation aimed to adjust the JWL parameters A, B, R_1, and R_2 to best match the experimental results from the 0.7 kg and 1.4 kg tests. The results from the 1.0 kg tests and 8 m pressure sensors were reserved for validation purposes.

Compared with the traditional way of determining the EOS through the cylinder test, this methodology offers several advantages, including reduced experimental effort, lower costs, shorter analysis times, and improved safety due to reduced handling of explosives. In addition, the iterative optimization combined with LS-DYNA and LS-OPT allows a systematic and reproducible calibration of the JWL parameters.

Satisfactory results were obtained for both peak pressure and the average of the positive phase, with deviations below ± 10 % in most cases. In the validation with the 1.0 kg tests, peak pressure deviations of −5.57 % and 10.81 % were observed at sensors located 2 and 4 meters from the charge, respectively. For the average positive phase, deviations of 6.21% and −3.7% were recorded at the same sensor positions.

The optimised JWL-EOS was then implemented in the Viper CFD software, where peak pressures and impulses were compared with experimental data across all tests and sensors, showing good agreement in both cases, with most relative errors below 10 %. However, this methodology has limitations in terms of validation. Future work should explore multi-geometric validation, multi-objective optimization, and uncertainty quantification. Additionally, alternative optimization strategies must be investigated to compare with the SRSM approach and establish a standardized methodology for explosive EOS calibration. Overall, the proposed methodology demonstrates a practical and accessible approach for EOS calibration, providing reliable results for PG3 under the

specific conditions studied in this work (spherical air detonations). At the same time, it lays the foundation for future research aimed at extending the methodology to more complex scenarios, such as non-spherical charges, surface-contact detonations, or confined explosions, through additional validation and model development.

CRediT authorship contribution statement

Angel Prado: Investigation, Methodology, Software, Visualization, Writing – original draft. **Ricardo Castedo:** Data curation, Resources, Software, Supervision, Writing – review & editing. **Anastasio P. Santos:** Conceptualization, Data curation, Project administration, Resources. **María Chiquito:** Software, Supervision, Validation, Writing – review & editing. **Carlos Gómez-De-Cabo:** Formal analysis, Software, Writing – review & editing. **Lina M. López:** Data curation, Supervision, Writing – review & editing. **José I. Yenes:** Software, Writing – review & editing.

Declaration of competing interest

The authors declare that they have no known competing financial interests or personal relationships that could have appeared to influence the work reported in this paper.

Acknowledgements

This research has been carried out under the Advance Kit of High ENergy Absorbing and lighT materials for side armor add-ONs to be used in military vehicles (No Main Battle Tanks) - AKHENATON project, funded by the Counter Improvised Explosive Devices Center of Excellence (C-IED CoE). Also, the authors acknowledge the institutional support RVO:61388998.

Data availability

Data will be made available on request.

References

[1] ANSYS Inc. (2024). AUTODYN User Manual (R2024 R2). https://www.ansys.com/products/structures/ansys-autodyn [accessed 12 November 2024].

[2] ANSYS Inc. (2025). LS-DYNA user manual (R15). https://www.ansys.com/products/structures/ansys-ls-dyna [accessed 12 November 2024].

[3] Lee, E. L., Hornig, H. C., & Kury, J. W. (1968). Adiabatic expansion of high explosive detonation products (No. UCRL-50422). Univ. of California Radiation Lab. at Livermore, Livermore, CA (United States). https://doi.org/10.2172/4783904

[4] Karlos, V., Solomos, G., & Larcher, M. (2016). Analysis of blast parameters in the near-field for spherical free-air explosions (JRC Technical Report EUR 27823 EN). Joint Research Centre; Publications Office of the European Union. https://doi.org/10.2788/778898

[5] Baranowski, P., Kucewicz, M., Pytlik, M., & Małachowski, J. (2022). Study of rock fracture under blast loading. Bull. Pol. Acad. Sci. Tech. Sci., 70(5). https://doi.org/10.24425/bpasts.2022.141723

[6] Bornstein, H., Kuznetsov, V., Lu, J. P., Stojko, S., & Freundt, J. (2022). Characterisation and validation of the JWL equation of state parameters for PE4. Int. J. Impact Eng., 164. https://doi.org/10.1016/j.ijimpeng.2022.104190

[7] Shin, H. S., Kim, S. W., Moon, J. H., & Park, G. K. (2024). Numerical Analysis of Blast Behavior for Non-ideal Explosive ANFO in Shock-Tube Test. Int. J. Concr. Struct. Mater., 18(1). https://doi.org/10.1186/s40069-024-00673-0

[8] Yi, C., Nyberg, U., Johansson, D., & San Miguel, C. R. (2024). Experimental and numerical investigation on nonideal detonation of aluminized emulsion explosives. Combust. Explos. Shock Waves, 60(5). https://doi.org/10.1134/S0010508224050137

[9] Kury, J. W., Hornig, H. C., Lee, E. L., McDonnel, J. L., Ornellas, D. L., Finger, M., Strange, F. M. & Wilkins, M. L. (1965). Metal acceleration by chemical explosives. In fourth symposium (International) on Detonation (pp. 3-13). US Government Printing Office Washington, DC.

[10] Sanchidrián, J. A., Castedo, R., Lopez, L. M., Segarra, P., & Santos, A. P. (2015). Determination of the JWL constants for ANFO and emulsion explosives from cylinder test data. Cent. Eur. J. Energetic Mater., 12(2).

[11] Cui, H., Song, P., Gu, X. H., Zhou, H., Xing, B. Y., Jiang, L., & Guo, R. (2020). Determination of the JWL parameters of detonation products using adaptive genetic algorithm. Propellants Explos. Pyrotech., 45(12). https://doi.org/10.1002/prep.202000148

[12] Kuznetsov, V. (2020). Determination of Gurney Quantities and JWL Equation of State Parameters from the Cylinder Expansion Test. Australia: Department of Defence Science and Technology Group, Australian Government.

[13] Liu, J., Xu, C., Han, X., Jiang, C., & Liu, G. (2016). Determination of the state parameters of explosive detonation products by computational inverse method. Inverse Probl. Sci. Eng., 24(1). https://doi.org/10.1080/17415977.2014.993981

[14] Sutton, B. D., Ferguson, J. W., & Hodgson, A. N. (2017, January). An analytical approach to obtaining JWL parameters from cylinder tests. In AIP Conference Proceedings 1793(1). AIP Publishing https://doi.org/10.1063/1.4971490

[15] Baust, T. M. (2020). Improving the Design and Evaluation of PDV-Based Cylinder Test Experiments for JWL-Parameter Determination. Propellants Explos. Pyrotech., 45(9). https://doi.org/10.1002/prep.202000002

[16] Li, X. L., Chen, K. Q., Huang, H. J., Yang, S., Song, Q. G., Cao, W., Lu, Z. H., Tian, C. & Hua, C., (2024). Automatic Optimization of JWL-Miller parameters of HMX-based aluminized explosive based on genetic algorithm. Propellants Explos. Pyrotech., 49(8). https://doi.org/10.1002/prep.202300195

[17] Itoh, S., Hamashima, H., Murata, K., & Kato, Y. (2002). Determination of JWL parameters from underwater explosion test. In 12th International Detonation Symposium, 281. Citeseer.

[18] Li, K., Dong, X., Li, X., Wang, Y., & Wang, W. (2021). Determination of JWL parameters from underwater explosion test of spherical explosives by continuous velocity probe. J. Energetic Mater., 39(4). https://doi.org/10.1080/07370652.2020.1822461

[19] Giam, A., Toh, W., & Tan, V. B. C. (2020). Numerical review of JWL parameters for TNT explosive in free-air blast. ASME J. Appl. Mech., 87(5). https://doi.org/10.1115/1.4046243

[20] Cooper, P. W. (1994). Comments on TNT equivalence (No. SAND-94-1614C; CONF-940776-6). Sandia National Labs., Albuquerque, NM (United States).

[21] Formby, S. A., & Wharton, R. K. (1996). Blast characteristics and TNT equivalence values for some commercial explosives detonated at ground level. J. Hazard. Mater., 50(2-3). https://doi.org/10.1016/0304-3894(96)01791-8

[22] Shirbhate, P. A., & Goel, M. D. (2020). A Critical Review of TNT Equivalence Factors for Various Explosives. Recent Advances in 182 Computational Mechanics and Simulations, 1(pp. 471-478). https://doi.org/10.1007/978-981-15-8138-0_36

[23] Baudin, G., & Serradeill, R. (2010). Review of Jones-Wilkins-Lee equation of state. In EPJ Web of Conferences, 10. https://doi.org/10.1051/epjconf/20101000021

[24] Lee, E. L., & Tarver, C. M. (1980). Phenomenological model of shock initiation in heterogeneous explosives. The Physics of Fluids, 23(12). https://doi.org/10.1063/1.862940

[25] Chiquito, M., Castedo, R., López, L. M., Santos, A. P., Mancilla, J. M., & Yenes, J. I. (2019). Blast wave characteristics and TNT equivalent of improvised explosive device at small-scaled distances. Def. Sci. J., 69(4). https://doi.org/10.14429/DSJ.69.13637

[26] Friedlander, F. G. (1946). The diffraction of sound pulses I. Diffraction by a semi-infinite plane. Proceedings of the Royal Society of London. Series A. Mathematical and Physical Sciences, 186(1006). https://doi.org/10.1098/rspa.1946.0046

[27] Rigby, S. E., Tyas, A., Bennett, T., Fay, S. D., Clarke, S. D., & Warren, J. A. (2014). A Numerical Investigation of Blast Loading and Clearing on Small Targets. Int. J. Prot. Struct., 5(3). https://doi.org/10.1260/2041-4196.5.3.253

[28] Kirchner, M. R., Kirchner, S. R., Dennis, A. A., & Rigby, S. E. (2024). Non-parametric characterization of blast loads. Int. J. Prot. Struct., 15(3). https://doi.org/10.1177/20414196231184581

[29] Castedo, R., Reifarth, C., Santos, A. P., Losada, J., López, L. M., Chiquito, M., & Mancilla, J. M. (2019). Application of grid convergence index to shock wave validated with LS-DYNA and ProsAir. Ingenieria e Investigacion, 39(3). https://doi.org/10.15446/ing.investig.v39n3.8138

[30] Donea, J., Huerta, A., Ponthot, J.-P., & Rodríguez-Ferran, A. (2004). Arbitrary Lagrangian-Eulerian Methods. The Encyclopedia of Computational Mechanics, Wiley, 1(14). https://doi.org/10.1002/0470091355.ecm009

[31] Lapoujade, V., Van Dorsselaer, N., Kevorkian, S., & Cheval, K. (2010). A study of mapping technique for airblast modelling. In Proc., 11th Int. LS-DYNA Users Conf. Livermore, CA: Livermore Software Technology Corporation, 5(pp. 5-32).

[32] Kalra, A., Zhu, F., Yang, K. H., & King, A. I. (2014). Key parameters in blast modeling using 2D to 3D ALE mapping technique. In Proc., 13th Int. LS-DYNA Users Conf. Livermore, CA: Livermore Software Technology Corporation.

[33] Bergh, M., Wedberg, R., & Lundgren, J. (2018). Optimization of equation of state and burn model parameters for explosives. In AIP Conference Proceedings 1979(1). AIP Publishing. https://doi.org/10.1063/1.5044875

[34] ANSYS Inc. (2020). LS-OPT User's Manual (Version 7.0). https://lsdyna.ansys.com/ls-opt/ [accessed 12 November 2024].

[35] Stirling, C. (2025). Viper Applied Science. Available at: https://www.viper.as/ [accessed 18 November 2025].

[36] Tyas, A., Reay, J. J., Fay, S. D., Clarke, S. D., Rigby, S. E., Warren, J. A., & Pope, D. J. (2016). Experimental studies of the effect of rapid afterburn on shock development of near-field explosions. International Journal of Protective Structures, 7(3). https://doi.org/10.1177/2041419616665931

[37] Schwer, L., & Rigby, S. (2018). Secondary and height of burst shock reflections: application of afterburning. Proceedings of the 25th Military Aspects of Blast and Shock (MABS25), The Hauge, Netherlands.